Size-controlled PtNi nanoparticles as highly efficient catalyst for hydrodechlorination reactions

*Macarena Munoz, Sebastian Ponce, Gui-Rong Zhang and Bastian J.M. Etzold**

Lehrstuhl für Chemische Reaktionstechnik
Friedrich-Alexander-Universität Erlangen-Nürnberg
91058 Erlangen, Germany

*Corresponding author: Prof. Bastian J.M. Etzold
Tel.: +49 (9131) 85 - 27430
Fax: +49 (9131) 85 - 27421
E-mail: bastian.etzold@fau.de

Keywords: PtNi nanoparticles; hydrodechlorination; PVP; particle size; magnetic catalyst; 4-chlorophenol.

Abstract

The application of size-controlled PtNi nanoparticles (NPs) as catalyst on the aqueous-phase hydrodechlorination (HDC) of 4-chlorophenol (4-CP) under ambient conditions (25 °C, 1 atm) has been investigated. NPs were synthesized as a co-reduction of both metals following a solvothermal method which allowed a proper control of the PtNi alloyed NP size in the range of 4.4 to 12.0 nm. To make the active sites of the nanoalloy accessible, the stabilizer poly(N-vinyl-2-pyrrolidone) was removed by washing of the NPs with H_2O_2/H_2SO_4. Evaluating the NP structure/composition influence on the activity, a clear synergic effect between Pt and Ni was found. In this sense, complete conversion of 4-CP was achieved in 1 h reaction time with the bimetallic NPs whereas only 70% was reached with the monometallic Pt counterpart (NP size = 12 nm, [Pt] = 80 mg L^{-1}, $[4\text{-CP}]_0$ = 78 μmol L^{-1}). That effect could be related to the higher resistance of PtNi nanoalloy against chlorine poisoning compared to the monometallic Pt. In fact, PtNi NPs showed a remarkable stability and negligible deactivation even after storing the catalyst one month in the reaction mixture, whereas for the monometallic Pt fully deactivation resulted. The structure-sensitivity of HDC with PtNi nanocatalysts was finally confirmed as the catalytic performance was clearly dependent on the size. A volcano plot like behaviour was obtained, being 5.5 nm the optimum size. PtNi-5.5 led to the complete conversion of 4-CP in 15 min at a HDC rate of 3.12 L min^{-1} g_{Pt}^{-1}.

1. Introduction

Catalytic hydrodechlorination (HDC) is considered as a suitable process for the treatment of wastewater containing organochlorinated pollutants [1, 2]. The main advantages for the application of HDC compared to other techniques are the ability to treat a wide range of concentrations, the mild operating conditions as well as the low reagent demand. Moreover, HDC allows the safe conversion of organochlorinated waste regardless of their chlorine content into value added products, which can be recovered and further reused or safely disposed to biological or oxidation treatments [1, 3].

Conventional HDC catalysts are based on noble metals, being Pd, Rh and Pt the most active ones [4-9]. They are usually prepared by impregnation onto a support, mainly activated carbon or alumina [2, 10-12], and submitted to calcination-reduction activation treatments. The inherent disadvantage associated with those catalysts is the poor controllability of metal particle sizes and distributions because of forced condensation of metal precursors on the support [13]. Taking into account that HDC is a structure-sensitive reaction [14-18], designing catalysts with well-defined nanoparticle size and size distribution is increasing in interest. So far, the structure-sensitivity of the HDC reaction has been studied over colloidal Pd and Rh nanoparticles (NPs) with well defined particle structures [16-18], which have received much more attention than Pt ones. The lack of studies with the latter could be related to its remarkably lower stability for this reaction [8, 19]. Molina et al (2014)[8] compared the activity and stability of Pt, Pd and Rh catalysts supported on pillared clays upon 4-chlorophenol (4-CP) HDC and demonstrated that Pt shows considerably lower resistance to chlorine than Pd and Rh.

Here we adapt the strategy of employing bimetallic catalysts to improve the activity and stability of Pt in the HDC reaction. The promotion of monometallic catalysts by addition of a second transition metal is receiving growing attention and successful combinations such as PdFe, RhFe or PdNi have been already proved in HDC reactions [13, 20-22]. Particularly, Ni systems, as less costly catalysts, represent a promising option due to their high resistance to halogen poisoning [20, 23, 24]. So far, PtNi bimetallic catalysts have been employed in the hydrogenation of benzene [25], maleic anhydride [26], α,β-

unsaturated aldehydes [27] or cellulose [28], outrunning the activity and stability of the monometallic counterparts, but the effect of Ni addition to Pt for the HDC was not reported up to now.

The aim of this work is to address the synthesis of size-controlled bimetallic PtNi NPs and their application in HDC. The evaluation of the their activity and stability compared to bare Pt NPs as well as comprehensive knowledge on how particle size influences the catalytic activity and selectivity would represent an important contribution to the state-of-the-art. 4-CP has been selected as target pollutant for HDC reactions as it is the most used among monochlorophenols [29] and also the most toxic one [30]. Chlorophenols are commercially important chemicals [31], whose presence in the aquatic environment has inevitably increased during the past few decades [32-35], involving serious implications for both the environment and public health.

2. Materials and methods

2.1. Materials

Platinum (II) acetylacetonate (98%, abcr GmbH) and nickel (II) acetylacetonate (95%, Sigma Aldrich) were used as precursors for the synthesis of the nanoparticles. Benzyl alcohol (>99%, Fluka), poly(N-vinyl-2-pyrrolidone) (PVP, MW = 10000, Sigma Aldrich) and aniline (>99.5%, Sigma Aldrich) were used as solvent, capping agent and reductant, respectively. The target pollutant tested in the HDC experiments was 4-chlorophenol (99%, Alfa Aesar). All the reagents were used as received without further purification.

2.2. Synthesis and characterization of PtNi nanoparticles

The synthesis of PtNi nanoparticles in average diameters of 4.4-12.0 nm was performed as a co-reduction of both metals following a solvothermal method. Briefly, nickel (II) and platinum (II) acetylacetonates and PVP were dissolved in a mixture of benzyl alcohol and aniline for 15 min under vigorous stirring at room temperature. The reaction mixture was then sealed in a PTFE-lined vessel and

heated in a furnace at temperatures within the range of 150-190 °C for different reaction times (6-15 h). The amount of precursor salts, capping and reducing agents was varied in order to learn the effect of these variables on the size and distribution of PtNi nanoparticles. After reaction, the reactor was cooled down to ambient temperature before opening. An excess of acetone (1:3, v/v) was then added to the reacted solution to precipitate the colloidal nanoparticles. Finally, they were purified by dispersion in a solution of ethanol/acetone (50-50%, v/v) by sonication, followed by centrifugation (6000 rpm during 10 min) and removal of the supernatant, which resulted in a PtNi NPs sludge redispersible in water and polar solvents. In order to evaluate the possible synergic effect between Pt and Ni in the HDC reaction, monometallic Ni and Pt NPs were also synthesized following the same procedure.

As will be described later, the NPs require further cleaning to be active in HDC. Thus, they were submitted to a cleaning procedure which allows the complete removal of PVP [36]. Hereby, the as-prepared NPs were suspended in a diluted Piranha solution (0.2 mL of 30 wt.% H_2O_2, 0.5 mL of H_2SO_4 (98%) and 7.3 mL of distilled water) and centrifuged at 6000 rpm for 15 min. Afterwards, the supernatant was removed and the remaining NPs were washed with ultrapure water to remove all the PVP in solution and the residual H_2O_2 and H_2SO_4.

Transmission electron microscopy (TEM) measurements were carried out using a Philips CM 300 UT microscope operated at 300 kV. The samples were prepared by placing a drop of colloidal nanoparticle suspension in deionized water onto a carbon film coated cooper grid, followed by drying at ambient conditions. Software “Nano Measurer 1.2” was used for measuring and counting the nanoparticles on digital TEM images (more than 200 nanoparticles were measured per sample).

2.3. HDC experiments

Catalytic HDC runs were carried out batch-wise in a magnetically stirred four-necked glass reactor (250 mL) equipped with a reflux condenser and temperature control. The reaction took place during 3 h under vigorous stirring (750 rpm) and continuous feeding of H_2 (50 NmL min^{-1}) at 25 °C. The starting

concentration of the target pollutant and the reaction volume were fixed at 78 μmol L^{-1} and 150 mL, respectively. Unless otherwise indicated, a Pt catalyst concentration of 80 mg L^{-1} was used. Blank experiments in the absence of hydrogen/catalyst were carried out achieving negligible adsorption/conversion values (<5%). Each HDC run was carried out by triplicate being the standard deviation less than 10% in all cases.

2.4. Analytical methods

The progress of the HDC reactions was followed by periodically withdrawing and analysing liquid samples from the reactor. 4-CP, phenol (Ph), cyclohexanone (C-one) and cyclohexanol (C-ol) were analysed by a gas chromatograph with a 25 m length x 0.32 mm i.d. capillary column (CP-FFAP CB, Varian) coupled to a flame ionization detector (GC 3900, Varian).

2.5. Calculation of the turnover frequency (TOF), 4-CP conversion and products selectivity

Turnover frequencies (TOF) for PtNi NPs were calculated in order to correct the activity for the dispersion of the metal using the following equation:

$$TOF\ (s^{-1}) = \frac{k_{HDC} \cdot [4CP]_0 \cdot M_{Pt}}{D \cdot 60} \times 100 \qquad (1)$$

where k_{HDC} denotes the first order rate constant for 4-CP HDC (L min^{-1} g_{Pt}^{-1}), $[4CP]_0$ – the initial 4-CP concentration (mol L^{-1}), M_{Pt} – the atomic mass of Pt (195.08 g mol^{-1}), and D – dispersion (%). The estimation of the dispersion was based on an onion-like magic cluster model as detailed in the Supplementary Material.

The conversion of 4-CP and the selectivity towards Ph, C-one and C-ol in the HDC of 4-CP were calculated in a molar basis as:

$$X_{4CP}\ (\%) = \frac{[4CP]_0 - [4CP]_t}{[4CP]_0} \times 100 \quad (2)$$

$$S_{Product}\ (\%) = \frac{[Product]_t}{[4CP]_0 - [4CP]_t} \times 100 \quad (3)$$

3. Results and discussion

3.1. Characterization of the nanoparticles

Detailed TEM characterization of the Pt, Ni and PtNi nanoparticles resulting at different synthesis conditions was carried out to determine the average particle size and distribution. The NPs are denoted as PtNi-α, Pt-α and Ni-α, where α indicates the mean size of the nanoparticles in nanometer (nm) and -nw if no washing for PVP removal was applied. Table 1 shows that for PtNi always narrow particle size distributions resulted and sizes from 4.4 to 12.0 nm can be employed for the study (see Figure S1 in the Supplementary Material for TEM images and particle size histograms). The variation of PVP and the reagent affect directly to the NPs size whereas reaction time and operating temperature have a major influence in the NPs size distribution. Pt could also be synthesized in a similar size whereas for pure Ni only larger nanoparticles could be prepared. As representative example, Figure 1a shows the TEM image, particle size distribution and interplanar distance of PtNi-5.5-nw NPs. It is important to highlight that all the NPs regardless of their composition or size, presented a well-defined truncated octahedral shape, which has proved to improve significantly their activity due to the presence of more favourable adsorption sites in the edges between (100)/(111) facets, compared to the state-of-the-art spherical NPs in other catalytic process such as oxygen reduction [37]. On the other hand, for the bimetallic PtNi NPs the measured interplanar distance confirms the presence of the PtNi nanoalloy (NiPt phase: d_{111} = 2.15 Å; Pt phase d_{111} = 2.26 Å; Ni phase d_{111} = 2.03 Å) [38].

As the presence of PVP on the surface of the NPs could influence their activity, a second set of NPs was post-treated to remove the capping agent. Several protocols for cleaning the NPs can be found in

the literature, most of them based on thermal and oxidative approaches [36, 39, 40]. In this work, we have followed the oxidative method reported by Monzo et al. (2012)[36], as it has proved to allow the removal of the capping agent without compromising the size and structure of Pt NPs. Figure 1b shows the TEM images of PtNi-5.5 NPs after the cleaning with H_2O_2/H_2SO_4 (see Figure S2 of the Supplementary Material for TEM images of monometallic NPs and bimetallic PtNi NPs of different sizes). As observed, the structure, size and distribution of the NPs was not significantly changed for all the NPs synthesized in this work regardless of their composition or size (Table 2). In the same line, the interplanar distance remained unchanged within the measurement error.

3.2. Activity and stability of monometallic and bimetallic nanoparticles

3.2.1. Effect of the capping agent

It is well-known that stabilizers interact with the surface of colloidal nanoparticles and can compete with reactants and products for the adsorption sites or preventing their accessibility and even modify the surface electronic structure of their stabilized metal nanoparticles [41], thus influencing their catalytic activity [42-47]. In this sense, experiments with PVP-stabilized NPs were carried out with the aim of addressing the effect of PVP on their HDC activity. Within 24 h reaction time the PVP-stabilized NPs showed negligible activity in the HDC of 4-CP regardless of their size or composition (Pt, PtNi) (see Figure S3 of the Supplementary Material for experimental data). In agreement with previous works [45, 48, 49], it can be concluded that PVP blocks the active sites and removal of the stabilizer is necessary to obtain catalytic activity.

The effect of removing PVP through a H_2O_2/H_2SO_4 treatment on the catalytic activity was studied for PtNi-5.5 NPs (Figure 2) and resulted in a significant improvement. After washing the NPs full conversion of 4-CP is achieved within 15 min whereas the non-washed NPs showed after 3 h a conversion of only 10%. In this sense, further testing of the NPs was carried out after their cleaning with H_2O_2/H_2SO_4.

3.2.2. Monometallic Pt and Ni vs. bimetallic PtNi nanoparticles

The catalytic activity of the monometallic Ni-42, Pt-12 and bimetallic PtNi-12 NPs were evaluated in the HDC of 4-CP. The activity profiles are depicted in Figure 3a. As can be seen, the monometallic Ni NPs displayed negligible conversion of 4-CP after 1 h reaction time. Apart from the considerably large Ni NPs tested, the complete absence of activity can be attributed to the mild operating conditions used in this work as it is known that Ni-based catalysts are not active in HDC unless the reaction is taking place at considerable high temperatures (100 – 350 °C) [23, 50-52] compared to noble metal counterparts. However, both PtNi and Pt showed pronounced activity. The synergic effect between both metals is clear, while with the bimetallic catalyst 100% degree of conversion was achieved after 1 h, only around 70% resulted with monometallic Pt. Although both catalysts showed quite similar initial reaction rates, monometallic Pt NPs displayed adverse catalytic stability during the course of reaction. In fact, for the monometallic NPs the reaction kinetics could be divided into two parts (Figure 3b). In the first 15 min the first order reaction rate constant k_1 was calculated to be 0.63 L $min^{-1}g_{Pt}^{-1}$, almost the same as the bimetallic PtNi NPs (k = 0.64 L $min^{-1}g_{Pt}^{-1}$). From that time until the end of the reaction, NPs seem to deactivate and the rate constant decreased significantly (k_2 = 0.14 L $min^{-1}g_{Pt}^{-1}$).

While a better performance of PtNi NPs can originate from electronic and/or geometric effects as well as the appearance of mixed oxide sites [13, 17, 53, 54], this result indicates that a main difference to monometallic Pt is within the stability of the materials. It is unclear if the sudden change in activity stems from a change in the mechanism, blocking of active sites or other deactivation mechanism. To get further insights how the activity of both catalysts changes with time, repetition experiments were carried out adding directly new reactant to the reaction mixture after each experiment. Additionally, the NPs were stored in the reaction medium for one month prior adding new reactant. Figure 4 shows the experimental HDC results for the three consecutive runs and that carried out after one month of nanoparticles exposure to the reaction medium. Monometallic Pt suffered a considerable fall in activity.

The two regions of different activity before and after 15 minutes of reaction time are still observable and the initial activity of the consecutive run is higher than the activity at the end of the previous experiment. Furthermore, a drop in 4-CP conversion of 70% results after 3 cycles and full deactivation of the Pt NPs after 1 month in contact with the reaction mixture. On the opposite, the bimetallic catalyst showed constant activity for all runs and no deactivation can be observed even after being exposed for 1 month to the reaction mixture. This remarkable stability of PtNi outruns the stability of well-known active and stable catalysts such as Rh in HDC, which have been usually preferred rather than Pt. E.g. Baeza et al. (2014)[17] applied colloidal size-controlled Rh NPs in the aqueous-phase HDC of 4-CP and observed a decrease on the HDC activity around 40% after three consecutive cycles. In the same line, the striking stability of PtNi nanoparticles is comparable to that shown by conventional HDC catalysts such as Pd supported on alumina, activated carbon or pillared clays upon long-term continuous experiments (100 h) [8, 14].

Main reasons for the deactivation of catalyst during HDC is seen in the surface poisoning by chloride ions from the couple product HCl, while metal loss or sintering could be discarded in most studies [8, 13, 19]. In this sense, the remarkably higher stability of the bimetallic PtNi NPs upon HDC could be related to the greater resistance of the alloy PtNi species to chlorine. This can stem from the influence of the alloying on the electronic properties of Pt, which altered in other reactions the chemisorption properties. E.g. the hydroxyl coverage on Pt is lowered during oxygen reduction reaction [37, 55]. Another mechanism could be the higher tendency of the base metal to attract chlorine and thus remove the adsorbed species from the neighbouring Pt [13, 20-22, 56].

Apart from chlorine induced deactivation the decrease of activity due to loss of NPs during recycling can be problematic and a proper retention and separation of the NPs is needed. Beside the economical point of view this is also requested for environmental aspects since NPs can cause toxic effects in living organisms and can act as pollutant carriers. In this sense, it is important to highlight that the bimetallic PtNi NPs synthesized in this work present magnetic properties, which allow their retention and fast

separation by the application of a magnetic field (see Figure S4 of the Supplementary Material for the image of the PtNi NPs suspended in water under a magnetic field).

3.3. Effect of PtNi NPs size on the activity and selectivity

Figure 5a shows the evolution of 4-CP upon HDC over the bimetallic PtNi NPs of different sizes in the range of 4.4 to 12.0 nm. With the exception of the size of 8.3 nm, the complete degradation of 4-CP was achieved in all cases. In agreement with previous results, the HDC of 4-CP follows a first order kinetics and the experimental results can be described in fairly good agreement (Figure S5 of the Supplementary Material shows the linear relationship between the obtained HDC rate constants with the PtNi NPs concentration). The structure-sensitivity of the reaction can be more clearly seen in Figure 5b, which depicts the HDC rate constant values *vs.* the PtNi NPs mean size. The activity shows a clear dependence on the size of the NPs, following a volcano plot like behaviour with the maximum value obtained at d = 5.5 nm. Increasingly higher sizes led to lower HDC activities. Reason is most likely the higher percentage of low coordinated sites (edge/corner positions) in the smaller NPs, which can act as active sites [17]. The slightly higher activity of PtNi-12 compared to PtNi-8.3 can be directly related to the presence of twinned defects in that structure due to the seed growing procedure applied in its synthesis. On the other hand, the higher solubility of hydrogen in larger particles must be also considered [16]. Although in a lower extent, NPs smaller than 5.5 nm also showed a poorer performance, which can be associated in this case to the increase of the adsorption energy of the reactants, favouring poisoning of the catalyst [17]. Similar conclusions have been reached by other authors dealing with both conventional [57-59] and size-controlled nanoparticle catalysts [16, 17]. Baeza et al. (2014)[17] found a similar behaviour for colloidal Rh NPs in the aqueous-phase HDC of 4-CP, being 2.8 nm the optimum NP size. The same authors also proved in a former work [16] that in the case of Pd the smallest NPs tested (2.8 nm) exhibited the highest activity values normalized to mass. Nevertheless, correcting the activity for the dispersion of the metal shows an increase in TOF with

decreasing particle size. Thus, an optimum particle size shall exist due to increasing intrinsic activity but also lower dispersion with bigger particles. In this work, the corrected activity per the amount of Pt present in the NPs surface showed the same behaviour previously described (Table 3) resulting in 5.5 nm as optimum NP size for the HDC of 4-CP with PtNi.

The obtained TOF values for PtNi NPs are somewhat lower than those reported in the literature for HDC of 4-CP with supported Pt catalysts at ambient temperature (0.31-1.26 x 10^{-2} s^{-1}). However, it is important to highlight that those catalysts showed very low dispersions of the active phase (6.3-15%), which explains that the activity per accessible atom of Pt is higher. In fact, if the total mass of Pt used in the experiments is considered, the colloidal PtNi-5.5 NPs prepared in this work showed a considerably higher HDC rate (3.12 L min^{-1} g_{Pt}^{-1} *vs.* 0.07-0.54 L min^{-1} g_{Pt}^{-1}) [8].

Figure 6 shows the selectivities towards Ph, C-one and C-ol *vs.* 4-CP conversion for the bimetallic PtNi NPs at different sizes. The results are consistent with a consecutive reaction pathway where 4-CP reacts with hydrogen to produce Ph, which is further hydrogenated to C-one, being the latter finally reduced to C-ol (Figure 7). The PtNi NPs size does not present a remarkable effect on the selectivity, as similar trends are observed by varying the size. However, it seems that sizes of 5.5 and 6.3 nm present a slightly higher hydrogenation activity as C-one starts to appear at very low conversion of 4-CP. In fact, if the selectivities obtained at the end of the reactions (3 h) are compared (Table 3), it is clear that the same behaviour described previously for the HDC activity can be also applied for the hydrogenation one. In this sense, PtNi5.5 shows the highest hydrogenation activity as Ph is completely degraded during the course of reaction obtaining C-one and C-ol as final products. In the same line, PtNi-4.4 and PtNi-6.3 NPs showed similar hydrogenation activities with a low selectivity to Ph at the end of the experiments. On the contrary, PtNi-8.3 presented the lowest hydrogenation activity with a high selectivity to Ph and complete absence of C-ol. According to its different structure, PtNi-12 showed a higher hydrogenation activity being C-one the major reaction product and also showing C-ol.

4. Conclusions

The application of Pt-based catalysts in aqueous-phase HDC reactions has received considerably lower attention compared to Pd or Rh ones, mainly due to its lower resistance towards chlorine poisoning and thus, its remarkably lower stability. In this work, it has been demonstrated that the incorporation of Ni to Pt is a proper strategy to significantly improve the stability of the catalyst. In this sense, whereas the monometallic Pt NPs were fully deactivated after being exposed for 1 month to the reaction mixture, the bimetallic PtNi ones maintained their high activity almost unchanged. The outstanding stability of the bimetallic catalyst can be related to the greater resistance of the PtNi alloy species to chlorine.

The performance of PtNi catalyst was significantly affected by the NP size, confirming the structure-sensitivity of the HDC reaction. As the size of PtNi NPs decreased the activity increased reaching a maximum at 5.5 nm whereas further decrease of the NP size led to a fall on the activity. Interestingly, the optimum PtNi-5.5 NPs showed a higher HDC rate than those previously reported in the literature for conventional supported Pt catalysts. On the other hand, the selectivity was also affected by the NP size. In this sense, PtNi-5.5 NPs showed also the highest hydrogenation activity, leading to the complete hydrogenation of phenol and obtaining cyclohexanone and cyclohexanol as final reaction products.

The results obtained in this work demonstrate that the stability of Pt catalysts can be remarkably improved by the addition of Ni whereas the activity and selectivity of the PtNi nanoalloy can be also appropriately tuned by controlling the nanoparticle size. Another interesting advantage of Ni addition is the appearance of magnetic properties on the NPs, which strongly facilitates their separation and recovery. These findings offer new perspectives for the design and optimization of active, easily-recoverable and durable Pt-bearing nanoparticle catalysts.

Figure and Table captions

Figure 1. Representative TEM images of PtNi-5.5 before (a) and after the cleaning with H_2O_2/H_2SO_4 (b). The insets show the lattice fringe spacing of the NPs and the NPs size distribution.

Figure 2. HDC of 4-CP over PVP-protected PtNi-5.5-nw NPs (open symbols) and cleaned PtNi-5.5 NPs (solid symbols) ([NPs] = 80 mg L^{-1}).

Figure 3. HDC of 4-CP over bimetallic PtNi-12 NPs (black squares) and monometallic Pt-12 NPs (grey circles) and Ni-42 (white triangles) (a). Fitting of 4-CP HDC bimetallic with PtNi-12 NPs and monometallic Pt-12 NPs to a first order reaction kinetic model (b) ([NPs] = 80 mg L^{-1}).

Figure 4. Evolution of 4-CP conversion upon HDC over bimetallic PtNi-12 NPs (a) and monometallic Pt-12 NPs (b) for three consecutive runs (1^{st}: black squares, 2^{nd}: open circles, 3^{rd}: open triangles) and for the experiment performed after one month (black stars) ([NPs] = 80 mg L^{-1}).

Figure 5. a: HDC of 4-CP over bimetallic PtNi NPs of different sizes: 4.4 (solid squares), 5.5 (open circles), 6.3 (solid triangles), 8.3 (open triangles) and 12.0 (solid stars) nm. Experimental (symbols) and predicted (solid lines) values. b: HDC rate constants *vs.* mean size of the bimetallic PtNi NPs.

Figure 6. Selectivity towards phenol (a), cyclohexanone (b) and cyclohexanol (c) *vs.* 4-CP conversion in HDC runs with the bimetallic PtNi NPs of different sizes: 4.4 (solid squares), 5.5 (open circles), 6.3 (solid triangles), 8.3 (open triangles) and 12.0 (solid stars) nm.

Figure 7. Reaction pathway for 4-CP HDC with PtNi nanoparticles.

Table 1. Resulting mean diameters (d_{NP}) and size distributions (σ_{NP}) for Pt, Ni and PtNi NPs at varying synthesis conditions.

Table 2. Mean diameter (d_{NP}) and size distribution (σ_{NP}) of Pt, Ni and PtNi NPs after the H_2O_2/H_2SO_4 cleaning treatment.

Table 3. TOF values for 4-CP HDC and products selectivity (%) at the end of the experiments (3 h) with the bimetallic PtNi NPs of different sizes.

Acknowledgments

The authors gratefully acknowledge the funding of the German Research Council (DFG), which, within the framework of its Excellence Initiative, supports the Cluster of Excellence "Engineering of Advanced Materials" (www.eam.uni-erlangen.de) at the University of Erlangen-Nürnberg.

References

[1] M.A. Keane, J. Chem. Technol. Biotechnol. 80 (2005) 1211–1222.

[2] M.A. Keane, ChemCatChem. 3 (2011) 800–821.

[3] M. Munoz, Z.M. de Pedro, J.A. Casas, J.J. Rodriguez, Appl. Catal., B 150–151 (2014) 197–203.

[4] S. Kovenklioglu, Z. Cao, D. Shah, R.J. Farrauto, E.N. Balko, AlChe J. 38 (1992) 1003–1012.

[5] Y. Ukisu, S. Kameoka, T. Miyadera, Appl. Catal., B 18 (1998) 273–279.

[6] Y. Shindler, Y. Matatov-Meytal, M. Sheintuch, Ind. Eng. Chem. Res. 40 (2001) 3301–3308.

[7] E. Díaz, J.A. Casas, A.F. Mohedano, L. Calvo, M.A. Gilarranz, J.J. Rodríguez, Ind. Eng. Chem. Res. 47 (2008) 3840–3846.

[8] C.B. Molina, A.H. Pizarro, J.A. Casas, J.J. Rodriguez, Appl. Catal., B 148–149 (2014) 330–338.

[9] Y. Ren, G. Fan, C. Wang, J. Hazard. Mater. 274 (2014) 32–40.

[10] G. Yuan, M.A. Keane, Appl. Catal., B 52 (2004) 301–314.

[11] L. Calvo, M.A. Gilarranz, J.A. Casas, A.F. Mohedano, J.J. Rodríguez, Ind. Eng. Chem. Res. 44 (2005) 6661–6667.

[12] M. Munoz, Z.M. de Pedro, J.A. Casas, J.J. Rodriguez, Appl. Catal., A 488 (2014) 78–85.

[13] N.S. Babu, N. Lingaiah, P.S. Prasad, Appl. Catal., B 111–112 (2012) 309–316.

[14] E. Diaz, A.F. Mohedano, J.A. Casas, L. Calvo, M.A. Gilarranz, J.J. Rodriguez, Appl. Catal., B 106 (2011) 469–475.

[15] S. Gómez-Quero, F. Cárdenas-Lizana, M.A. Keane, Chem. Eng. J. 166 (2011) 1044–1051.

[16] J.A. Baeza, L. Calvo, M.A. Gilarranz, A.F. Mohedano, J.A. Casas, J.J. Rodriguez, J. Catal. 293 (2012) 85–93.

[17] J.A. Baeza, L. Calvo, M.A. Gilarranz, J.J. Rodriguez, Chem. Eng. J. 240 (2014) 271–280.

[18] J.A. Baeza, L. Calvo, J.J. Rodriguez, E. Carbó-Argibay, J. Rivas, M.A. Gilarranz, Appl. Catal., B 168–169 (2015) 283–292.

[19] Y. Hashimoto, Y. Uemichi, A. Ayame, Appl. Catal., A 287 (2005) 89–97.

[20] M.A. Keane, Appl. Catal., A 271 (2004) 109–118.

[21] E.V. Golubina, E.S. Lokteva, V.V. Lunin, N.S. Telegina, A.Y. Stakheev, P. Tundo, Appl. Catal., A 302 (2006) 32–41.

[22] I.A. Witońska, M.J. Walock, M. Binczarski, M. Lesiak, A.V. Stanishevsky, S. Karski, J. Mol. Catal. A: Chem. 393 (2014) 248–256.

[23] E. Shin, M.A. Keane, Chem. Eng. Sci. 54 (1999) 1109–1120.

[24] G. Tavoularis, M.A. Keane, J. Chem. Technol, Biotechnol. 74 (1999) 60–70.

[25] N.H.H. Abu Bakar, M.M. Bettahar, M. Abu Bakar, S. Monteverdi, J. Ismail, M. Alnot, J. of Catal. 265 (2009) 63–71.

[26] J. Li, W.P. Tian, L. Shi, Catal. Lett. 141 (2011) 565–571.

[27] Z. Jiang, Y. Zhao, L. Kong, Z. Liu, Y. Zhu, Y. Sun, ChemPlusChem 79 (2014) 1258–1262.

[28] G. Liang, L. He, M. Arai, F. Zhao, ChemSusChem. 7 (2014) 1415–1421.

[29] P.D. Warrington, British Columbia, Canada. (1997).

[30] M. Munoz, Z.M. de Pedro, J.A. Casas, J.J. Rodriguez, J. Hazard. Mater. 190 (2011) 993–1000.

[31] F.J. Urbano and J.M. Marinas, J, Mol. Catal. A: Chem. 173 (2001) 329–345.

[32] P. Lampi, T. Vartiainen, J. Toumisto, A. Hesso, Chemosphere 20 (1990) 625–634.

[33] M. Czaplicka, Sci. Total Environ. 322 (2004) 21–39.

[34] Y. Persson, A. Shchukarev, L. Öberg, M. Tysklind, Environ. Sci. Pollut. Res. 15 (2008) 463–471.

[35] M.J. Gómez, S. Herrera, D. Solé, E. García-Calvo, A.R. Fernández-Alba, Anal. Chem. 83 (2011) 2638–2647.

[36] J. Monzo, M.T.M. Koper, P. Rodriguez, ChemPhysChem 13 (2012) 709–715.

[37] C. Cui, L. Gan, H.H. Li, S.H. Yu, M. Heggen, P. Strasser, Nano letters. 12 (2012) 5885–5889.

[38] J. Arenas-Alatorre, M. Avalos-Borja, G. Díaz, Appl. Surf. Sci. 189 (2002) 7–17.

[39] C. Aliaga, J.Y. Park, Y. Yamada, H.S. Lee, C.K. Tsung, P. Yang, G.A. Somorjai, J. Phys. Chem. 113 (2009) 6150–6155.

[40] L.R. Baker, G. Kennedy, J.M. Krier, M. Van Spronsen, R.M. Onorato, G.A. Somorjai, Catal. Lett. 142 (2012) 1286–1294.

[41] G.R. Zhang and B.Q. Xu, Nanoscale. 2 (2010) 2798–2804.

[42] K.M. Bratlie, H. Lee, K. Komvopoulos, P. Yang, G.A. Somorjai, Nano letters. 7 (2007) 3097–3101.

[43] A. Villa, D. Wang, D.S. Su, L. Prati, ChemCatChem 1 (2009) 510–514.

[44] J.N. Kuhn, C. Tsung, W. Huang, G.A. Somorjai, J. Catal. 265 (2009) 209–215.

[45] A. Quintanilla, V.C.L. Butselaar-Orthlieb, C. Kwakernaak, W.G. Sloof, M.T. Kreutzer, F. Kapteijn, J. Catal. 271 (2010) 104–114.

[46] J.A. Lopez-Sanchez, N. Dimitratos, C. Hammond, G.L. Brett, L. Kesavan, S. White, P. Miedziak, R. Tiruvalam, R.L. Jenkins, A.F.Carley, D. Knight, C.J. Kiely, G.J. Hutchings, Nat. Chem. 3 (2011) 551–556.

[47] Y. Zhao, J.A. Baeza, N. Koteswara Rao, L. Calvo, M.A. Gilarranz, Y.D. Li, L. Lefferts, J. Catal. 318 (2014) 162–169.

[48] Y. Li, M.A. El-Sayed, J. Phys. Chem. B 105 (2001) 8938–8943.

[49] J.Y. Park, C. Aliaga, J.R. Renzas, H. Lee, G.A. Somorjai, Catal. Lett. 129 (2009) 1–6.

[50] M.A. Keane, G. Pina, G. Tavoularis, Appl. Catal., B 48 (2004) 275–286.

[51] P. Kim, J.B. Joo, H. Kim, W. Kim, Y. Kim, I.K. Song, J. Yi, Catal, Lett. 104 (2005) 181–189.

[52] N. Wu, W. Zhang, B. Li, C. Han, Microporous and Mesoporous Materials. 185 (2014) 130–136, doi: http://dx.doi.org/10.1016/j.micromeso.2013.11.017.

[53] N.S. Babu, J. Lingaiah, K. Vinod, P.S. Prasad, Appl. Catal., A 367 (2009) 70–76.

[54] H.L. Jiang and Q. Xu, J. Mater. Chem. 21 (2011) 13705–13725.

[55] V.R. Stamenkovic, B. Fowler, B.S. Mun, G. Wang, P.N. Ross, C.A. Lucas, N.M. Markovic, Science 315 (2007) 493–497.

[56] Y. Cesteros, P. Salagre, F. Medina, J.E. Sueiras, Appl. Catal., B 25 (2000) 213–227.

[57] S. Gómez-Quero, F. Cárdenas-Lizana, M.A. Keane, Ind. Eng. Chem. Res. 47 (2008) 6841–6853.

[58] I. Witonska, A. Krolak, S. Karski, J. Mol. Catal. A, 331 (2010) 21–28.

[59] I. Witonska, M.J. Walock, P.. Dziugan, S. Karski, A.V. Stanishevsky, Appl. Surf. Sci. 273 (2013) 330–342.

Table 1

Table 1. Resulting mean diameters (d_{NP}) and size distributions (σ_{NP}) for Pt, Ni and PtNi NPs at varying synthesis conditions.

Nanocatalyst	Pt (mg)	Ni (mg)	Benzyl alcohol (mL)	PVP (mg)	Aniline (mL)	T (°C)	time (h)	d_{NP} (nm)	σ_{NP} (nm)
Pt-12-nw	26.6	0.0	10	160	0.2	150	15	12.4	2.0
Ni-42-nw	0.0	26.6			0.2			42.0	10.8
PtNi-4.4-nw	16.0	10.3		320	0.2			4.4	0.8
PtNi-5.5-nw				160	1.0			5.5	0.9
PtNi-6.3-nw					0.2			6.3	0.8
PtNi-8.3-nw	32.0	20.6		320	0.2	190	6	8.3	1.0
PtNi-12-nw *								12.0	1.0

*PtNi-12 NPs were synthesized applying a seed-mediated growth procedure. It follows the same method as PtNi-8.3 but includes a second step where the reacted NPs are mixed with 5 mL of non-reacted solution and are submitted to the thermal treatment.

Table 2

Table 2. Mean diameter (d_{NP}) and size distribution (σ_{NP}) of Pt, Ni and PtNi NPs after the H_2O_2/H_2SO_4 cleaning treatment.

Nanocatalyst	d_{NP} (nm)	σ_{NP} (nm)
Pt-12	13.1	2.6
PtNi-4.4	5.8	0.6
PtNi-5.5	6.1	1.0
PtNi-6.3	7.3	1.0
PtNi-8.3	9.9	1.3
PtNi-12	12.6	2.2

Table 3

Table 3. TOF values for 4-CP HDC and products selectivity (%) at the end of the experiments (3 h) with the bimetallic PtNi NPs of different sizes.

Catalyst	TOF x 10^2 (s^{-1})	S_{Ph}	$S_{C\text{-}one}$	$S_{C\text{-}ol}$
PtNi-4.4	0.16	12	70	18
PtNi-5.5	0.30	0	70	30
PtNi-6.3	0.11	9	69	22
PtNi-8.3	0.05	60	40	0
PtNi-12	0.12	31	60	9

Figure 1

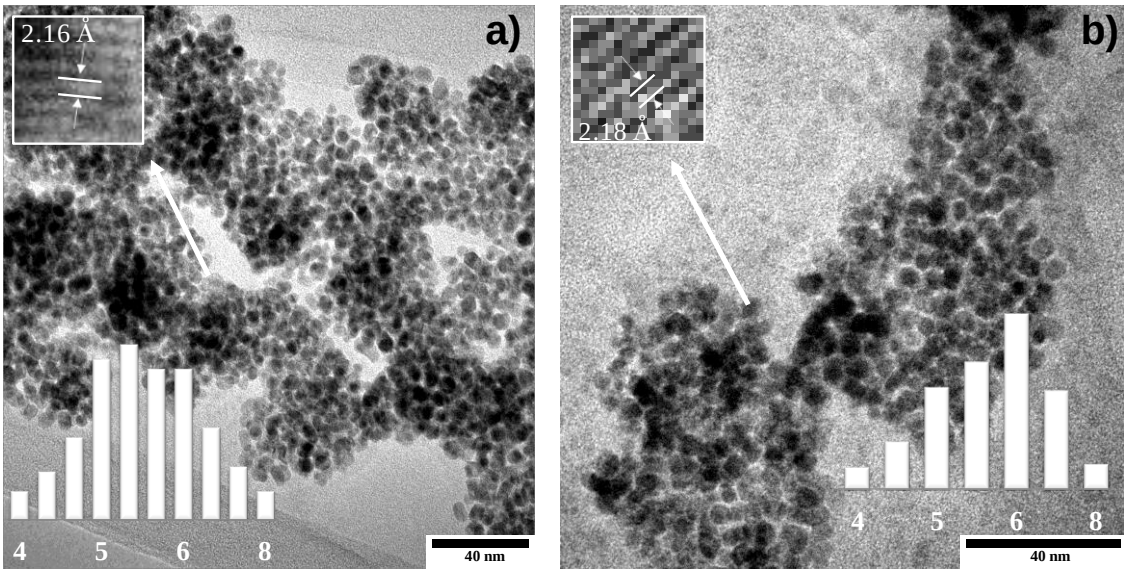

Figure 2

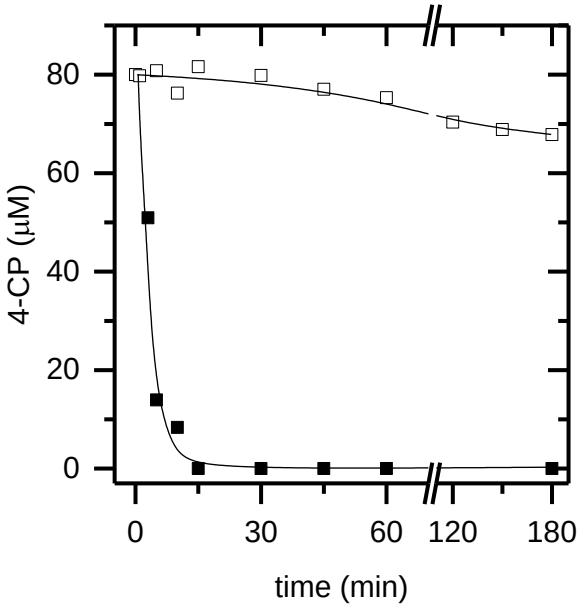

Figure 3

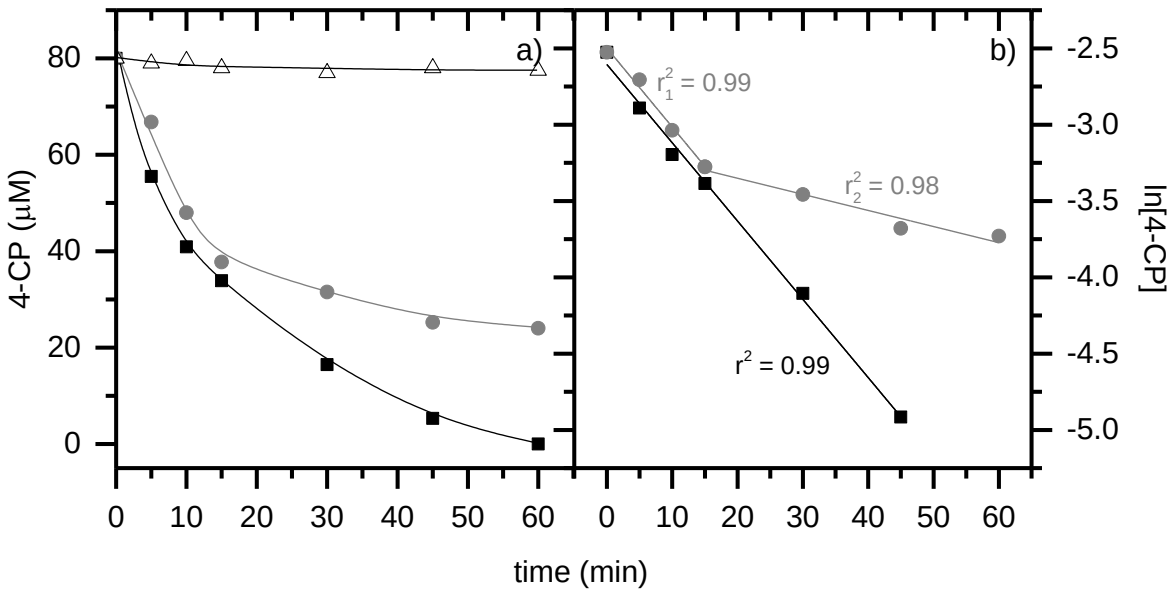

Figure 4

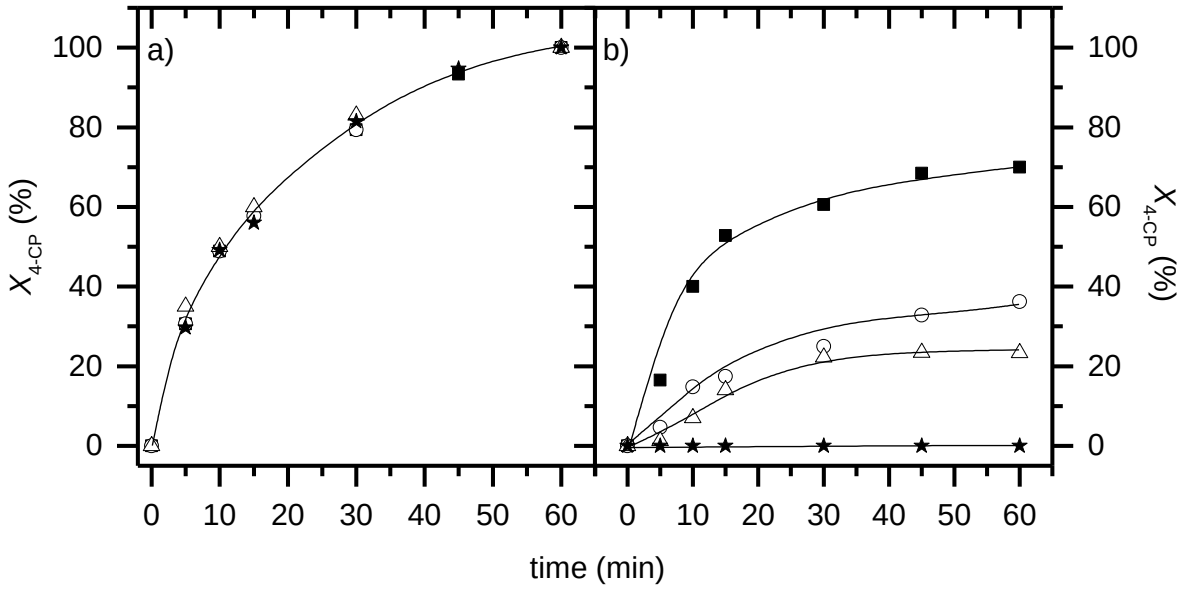

Figure 5

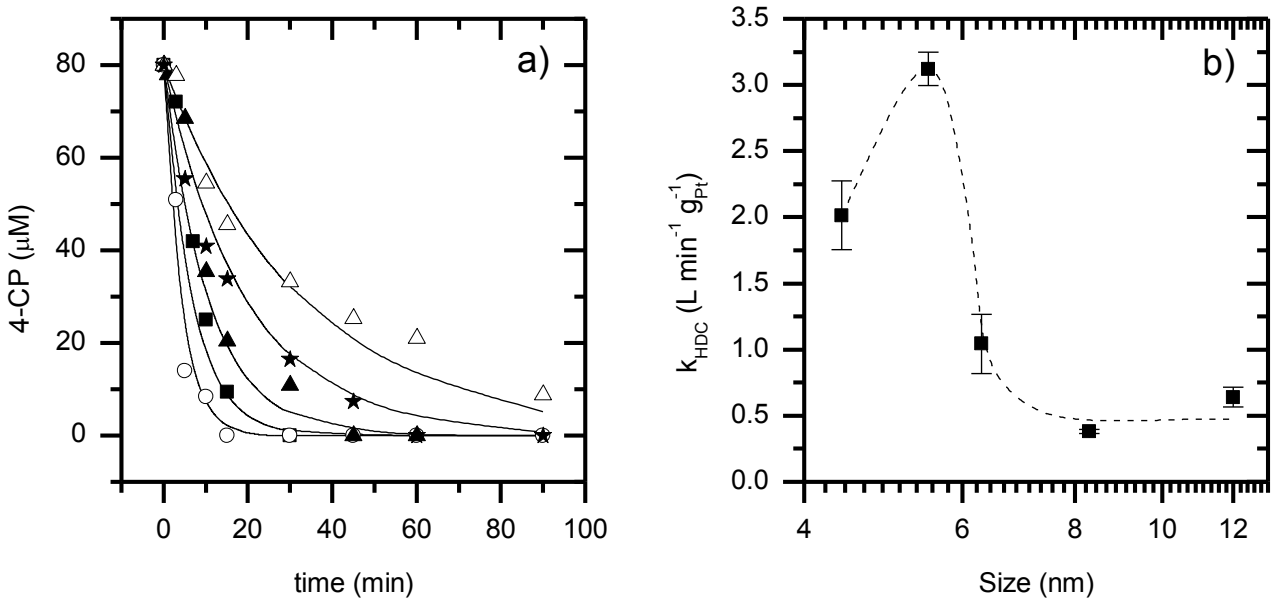

Figure 6

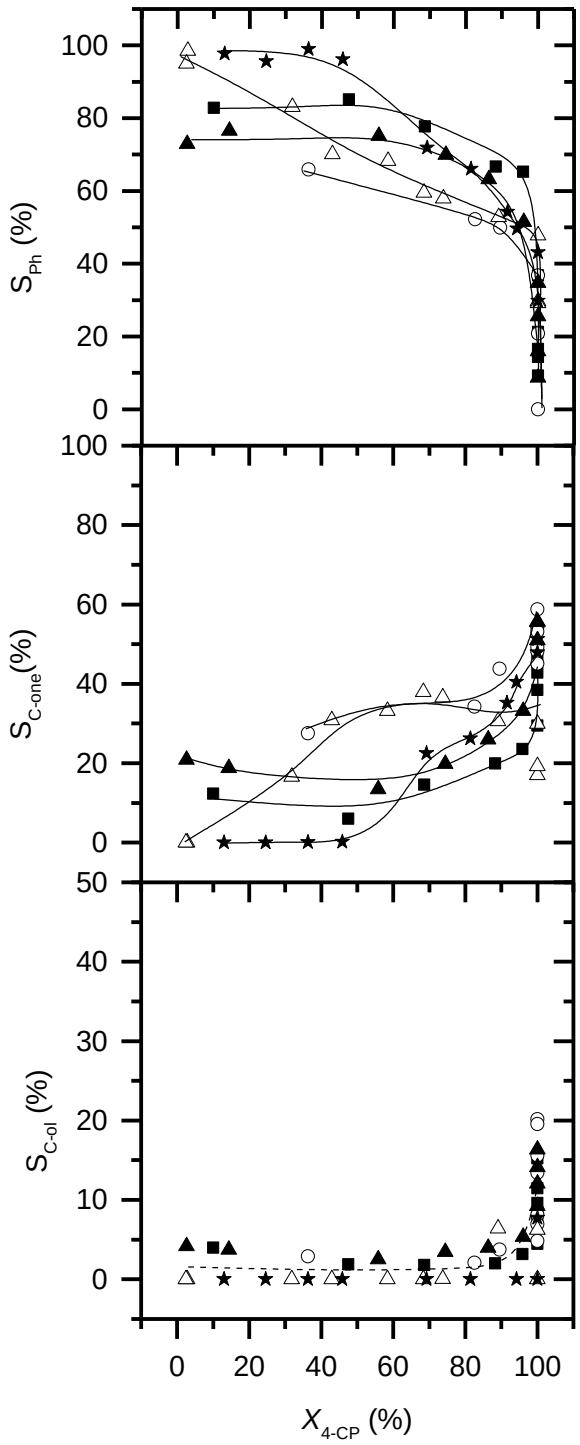
100
80
60
40
20
0
S_{Ph} (%)
100
80
60
40
20
0
S_{C-one}(%)
50
40
30
20
10
0
S_{C-ol} (%)
0
20
40
60
80
100
X_{4-CP} (%)

Figure 7